AIAA JOURNAL
Vol. 42, No. 5, May 2004

Reduced Flow of a Metastable Layer at a Two-Phase Limit

G. F. Naterer*
University of Manitoba, Winnipeg, Manitoba R3T 2N2, Canada

A solution procedure is outlined for predicting stable and metastable thermodynamic states, simultaneously, within a flowing supercooled surface film along an ice surface. This procedure involves a derived freezing fraction of incoming droplets in three-phase conditions, together with volume averaging to accommodate the momentum balance of the flowing surface layer. It is shown that this approach yields the proper trends when the flow temperatures are lowered sufficiently toward a two-phase limit. In this way, it provides a single parameter over the range between two-phase (rime ice) and three-phase (glaze ice) conditions. Also, it permits film flow calculations below and/or above the phase change temperature. As a result, an Eulerian volume averaging approach can be successfully applied to problems involving impinging droplets and glaze ice, which have generally been solved previously by Lagrangian methods. The numerical analysis is based on a control-volume-based finite element method. The predicted results are successfully validated through comparisons with analytical solutions and measured data.

Nomenclature

B = thickness of ice
b = thickness of water layer
C = phase volume fraction
e_0 = vapor pressure constant
$\hat{e}$ = internal energy
G = liquid water content
$\hat{G}$ = Gibbs free energy
h = convection coefficient
k = thermal conductivity
L = latent heat of fusion
M = film temperature gradient
m = mass
$\dot{m}''$ = interphase mass flux
n = freezing fraction
$\boldsymbol{q}$ = heat flux
S = source term, surface
T = temperature
u, v = velocity components
V = total velocity magnitude
$\mathcal{V}$ = volume
x, y = Cartesian coordinates
α = general scalar quantity
β = collection efficiency
ν = kinematic viscosity
ρ = density
τ = shear stress
χ = evaporation coefficient

Subscripts

a = air
B^+ = interface (film side)
B^- = interface (ice side)
e = energy, evaporation
f = phase change point
i = ice
k = phase
l = liquid
m = metastable
R = runoff
s = surface
w = water, wall
x, y = coordinate directions

Received 23 September 2002; revision received 11 June 2003; accepted for publication 12 August 2003.

*Associate Professor, Department of Mechanical and Industrial Engineering, 15 Gillson Street. Member AIAA.

I. Introduction

MULTIPHASE flows with impinging droplets on a flowing surface film arise in several engineering technologies.[1] Some important examples include de-icing of aircraft and power lines, microcasting shape deposition manufacturing (SDM), thin films manufactured for improved surface corrosion resistance, fuel sprays impinging and disintegrating along combustion chamber walls, and spray cooling of metal castings and extrusions. In the icing example, the impinging droplets impart the latent heat of phase change at the advancing ice interface. As a result, this energy transfer and other heating modes may heat the ice surface sufficiently to sustain a flowing supercooled surface layer. In that case, glaze ice (or wet ice) occurs, whereby the ice and unfrozen water layers grow simultaneously. In contrast, during the formation of rime ice (or dry ice), incoming droplets are solidified immediately on impact on the ice surface. An overview of aircraft icing processes has been documented by Bragg.[2] In this paper, the dynamics of the flowing supercooled liquid film, during glaze ice growth, is investigated numerically.

Glaze ice growth involves multiphase flow with one dispersed (droplet) phase and three continuous phases, that is, air, flowing surface layer, and solid (ice). Predictions of the air and droplet phase motions have been presented by Tsuboi and Kimura[3] for flows past circular conductors. Once deposited on the ice surface, the impinging solidified droplets alter the surface shape.[4] Runback flow of the supercooled liquid film depends on the external airstream at the water/air interface.[5] The heat balance within the unfrozen layer involves convection, conduction, heat extracted by the supercooled droplets, and other modes.[1,6] Unlike rime ice, which only requires consideration of the mass balance of incoming droplets,[7] the study of glaze ice growth involves coupled mass and heat balances, together with the momentum equation for the flowing surface layer.

Various flow regimes exist within the supercooled surface layer. A transition occurs between a smooth wet zone of unfrozen water and a rough zone with horn-shaped elements. This transition point may move upstream due to the formation of surface water beads, which are controlled by film flow in the smooth zone.[8] Measurements of glaze ice processes can be performed by an ultrasonic pulse-echo technique.[9] Based on this technique, measurements involving the formation of surface water beads, and movement of the smooth zone over time, can be gathered. In the presence of unfrozen water

along the ice surface, the echo patterns for glaze ice and rime ice are different. Rime ice yields a single echo, whereas glaze ice gives a series of rapidly varying echos returned back to the transducer. Applications of this technique in aircraft icing have demonstrated the movement of the wet/dry ice growth transition with time, indicating that a unified computational approach is warranted.

The impinging supercooled droplets on the flowing supercooled film exist at temperatures below the equilibrium freezing point.[10] Such conditions are called metastable. A system is considered to be in stable equilibrium if it has the lowest possible (global minimum) Gibbs free energy $\hat{G}$. However, there can be a variety of possible arrangements of atoms in the supercooled liquid, including an arrangement with a global minimum $\hat{G}$ (stable equilibrium), or others with local minima (metastable). Some metastable states can exist almost indefinitely, such as supercooled water, because of the presence of a free energy hump between the metastable and stable states. In the study of kinetics of transformation rates, higher energy barriers of $\hat{G}$ lead to slower transformation rates. Although phase change modeling is well understood for stable equilibrium states, such modeling and thermodynamics of metastable flowing liquids are not well understood in the technical literature.

In this paper, the supercooled droplets impinging on the flowing surface film are modeled by volume averaging, including compensation for the metastable conditions. The purpose of this paper is to show that this new formulation obeys certain asymptotic trends required under low-temperature conditions (rime ice). Rather than separate algorithms for rime and glaze ice, it provides film flow modeling over the entire range. In particular, this involves a new capability of volume averaging with liquid temperatures below 0°C (metastable) and above 0°C (stable), simultaneously. Predicted results are successfully compared with analytical and measured data. In contrast to explicit tracking of the moving phase interface(s), it is anticipated that the new formulation can yield computational savings (time and storage) due to the volume averaging procedures therein.

II. Problem Formulation

A volume averaged quantity in multiphase flow is defined as[1]

$$\langle \alpha_k \rangle = \frac{1}{\mathcal{V}_k} \int_{\mathcal{V}_k} \alpha_k \, d\mathcal{V} \tag{1}$$

where the subscript k refers to phase k, such as liquid (droplet) or gas (air). The volume occupied by phase k, within a control volume consisting of multiple phases, is denoted by $\mathcal{V}_k$. Also, the phase volume fraction can be written as

$$C_k = \mathcal{V}_k / \mathcal{V} \tag{2}$$

Furthermore, the liquid water content (LWC) is defined as

$$\hat{\rho}_l = m_l / \mathcal{V} = C_k \langle \rho_k \rangle \tag{3}$$

This variable refers to the mass of droplets per unit volume of the water/air mixture. It is usually expressed in units of grams per cubic meter. The local LWC is denoted by $\hat{\rho}_l$, whereas the freestream LWC is denoted by G. The local LWC is tracked spatially throughout the flowfield based on the volume averaged continuity equation for droplets,[4] so that the droplet fraction within each finite volume can be determined. On the other hand, the freestream LWC refers to the incoming value specified at the inlet boundary, and it is usually assumed to be constant in the numerical simulations. This freestream LWC typically depends on altitude, particularly with in-flight icing through clouds. For example, cirrus clouds typically contain less water than stratus, due to different cloud condensation mechanisms therein. Also, in-flight icing of aircraft usually involves much smaller droplets than ground-based icing of structures, such as freezing rain on overhead power transmission lines.

The governing equations for multiphase flow with droplets can be represented by the following volume averaged mass, x momentum and thermal energy equations[4,11]:

$$\frac{\partial \hat{\rho}_k}{\partial t} + \frac{\partial (\hat{\rho}_k u_k)}{\partial x} + \frac{\partial (\hat{\rho}_k v_k)}{\partial y} = 0 \tag{4}$$

$$\frac{\partial (\hat{\rho}_k u_k)}{\partial t} + \frac{\partial (\hat{\rho}_k u_k u_k)}{\partial x} + \frac{\partial (\hat{\rho}_k u_k v_k)}{\partial y} + \langle \dot{m}''_k u_k \rangle = C_k \langle G_{x,k} \rangle \tag{5}$$

$$\frac{\partial (\hat{\rho}_k \hat{e}_k)}{\partial t} + \frac{\partial [\hat{\rho}_k (\hat{e}_k u_k + q_{k,x})]}{\partial x} + \frac{\partial [\hat{\rho}_k (\hat{e}_k v_k + q_{k,y})]}{\partial y} = C_k \langle \hat{S}_{k,e} \rangle \tag{6}$$

where individual variables are defined in the Nomenclature.

These equations represent the governing equations for the external mulitphase flow, whereas an additional near-wall equation is needed for the flowing supercooled surface layer. In this article, a thin film approximation of the momentum balance is adopted therein.[1] This approximation yields a linear velocity profile within the unfrozen water layer (Fig. 1), that is,

$$u = \tau y / (\rho_w \nu_w) \tag{7}$$

where the shear stress at the water/air interface, τ, is specified based on experimental data.[12] Once the phase fraction of flowing liquid is obtained (next section), it is combined with Eq. (7) to determine the runback flow of water. This runback flow represents a portion of liquid mass transferred between elements along the moving boundary of the ice surface (Fig. 1).

To accommodate stable and metastable states of the flowing surface film simultaneously, a freezing fraction of incoming droplets will be developed. During the period of glaze ice growth, the conservation of mass involves the change of both ice and unfrozen water layers, that is,

$$\rho_i \frac{\partial B}{\partial t} + \rho_w \frac{\partial b}{\partial t} = \beta V G \tag{8}$$

This equation requires the proportion of droplets impinging on the ice surface to either contribute to the growth of solid ice $B(t)$ or to the unfrozen water layer $b(t)$.

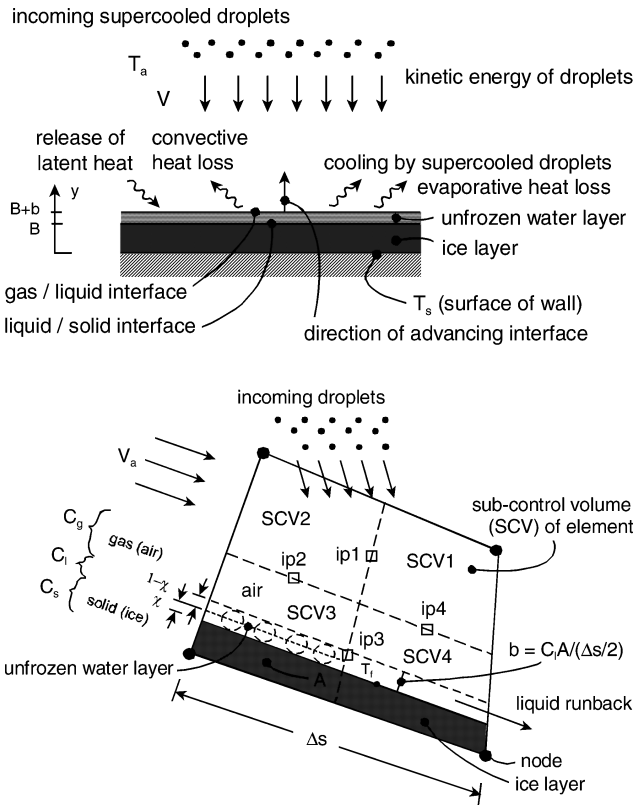

Fig. 1 Problem schematic with finite element discretization.

Rearranging Eq. (8), the fraction of incoming droplets that freeze n becomes

$$n \equiv \frac{\rho_i(\partial B/\partial t)}{\beta V G} = 1 - \frac{\rho_w(\partial b/\partial t)}{\beta V G} \tag{9}$$

This fraction is a bounded quantity ($0 \le n \le 1$). In Eqs. (8) and (9), the collection efficiency β represents the ratio of impinging droplet influx to the mass influx that would occur on the surface if the droplets were not deflected by the airstream.

When the heat balance is applied at the phase interface, the direction perpendicular to the interface must be defined for calculations of the heat flows (y direction) (Fig. 1). When a local heat balance at the interface between the ice and unfrozen water layer ($y = B$) is considered,

$$\rho_i L \frac{\partial B}{\partial t} = k_i \frac{\partial T_i}{\partial y}\bigg|_{B^-} - k_w \frac{\partial T_w}{\partial y}\bigg|_{B^+} \tag{10}$$

The notations B^- and B^+ refer to the ice and unfrozen water sides of the phase interface. Also, the subscripts i and w refer to ice and unfrozen water, respectively.

When Eq. (10) is substituted into Eq. (9),

$$n = \frac{\rho_i}{\beta V G}\left\{\frac{k_i}{\rho_i L}\frac{\partial T_i}{\partial y}\bigg|_{B^-} - \frac{k_w}{\rho_i L}\frac{\partial T_w}{\partial y}\bigg|_{B^+}\right\} \tag{11}$$

This result needs an explicit expression for the temperature gradient within the unfrozen layer, denoted by $(\partial T_w/\partial y)$.

The sign of this temperature gradient (positive or negative) depends on the thermodynamic state of the unfrozen layer. The interface temperature is considered to be the equilibrium phase change temperature (0°C), and so a negative sign suggests a subzero temperature and a nonequilibrium state within the layer. However, actual thermal conditions within the layer are difficult to predict conclusively, due to the lack of past experimental data therein and difficulties of measuring temperatures within this thin layer. Thus, certain insight regarding whether the predicted conditions are possible and irreversible, based on the second law, would be useful. However, the second law involves total entropy, including the system and surroundings, which requires detailed knowledge of the (unknown) surrounding heat flows.

Thus, it is preferable to use a state function that depends only on the system. The Gibbs free energy $\hat{G}$ is an example of a suitable state function. It can give useful insight into the existence of the nonequilibrium state of the unfrozen water. It can be shown that the Gibbs free energy $\hat{G}$ of the current system implies that freezing of the supercooled water occurs spontaneously, thereby entailing an irreversible process (see Appendix). Any other assumptions regarding the sign of the film temperature gradient would require a nonspontaneous or reversible process, in violation of the second law for the currently assumed conditions.

The temperature gradient in Eq. (11) can be estimated from a heat balance at the outer edge of the unfrozen water layer ($y = B + b$), that is,

$$-k_w \frac{\partial T_w}{\partial y}\bigg|_{B+b} = h(T_f - T_a) + \beta V G c_w (T_f - T_a) + \chi_e e_0 (T_f - T_a) - \frac{1}{2}\beta G V^3 \tag{12}$$

where the individual terms represent (from left to right) heat conduction within the unfrozen layer, convection, cooling by incoming supercooled droplets, evaporative heat loss, and kinetic energy of incoming droplets.

Substitution of the temperature gradient from Eq. (12) into Eq. (11) gives

$$n = \frac{1}{\beta V G L}\left\{k_i \frac{\partial T}{\partial y}\bigg|_{B^-} + h(T_f - T_a) + \beta V G c_w (T_f - T_a) + \chi_e e_0 (T_f - T_a) - \frac{1}{2}\beta G V^3\right\} \tag{13}$$

which gives the freezing fraction of incoming droplets. This fraction represents a fraction of latent heat released n that is needed to raise the ice temperature up to T_f, thereby sustaining the unfrozen water layer and glaze ice. The remaining fraction, $1 - n$, represents the proportion of droplet influx that does not immediately freeze on impact, but rather flows along the ice surface in the unfrozen water layer. In Eq. (13), an evaporation coefficient of $\chi_e = 8.52$ m/s (Ref. 13) will be used.

It will be shown that this formulation of phase change allows the numerical model to accommodate both stable and metastable states, simultaneously, in the flowing surface film. When some portion of the incoming droplets are solidified in Eq. (13), the solid phase is in stable equilibrium. If the Gibbs free energy was evaluated for all conceivable configurations of atoms in the liquid and solid phases, the most stable configuration would be the solid phase, when the temperature is below the equilibrium phase change point. This phase would have the lowest Gibbs free energy $\hat{G}$, and it represents the stable equilibrium phase. However, the other fraction, n in Eq. (13), is metastable in the liquid phase because it exists at a local minimum of $\hat{G}$, rather than the global minimum. The temperature of impinging droplets on the flowing surface layer is below the equilibrium phase change point. As a result, the formulation covers the range of both stable and metastable states.

Note that Eq. (13) leads to the proper limiting trends as $n \to 0$ and $n \to 1$, respectively. In particular, the numerical studies will show that all incoming liquid arrives and flows off of the surface when the droplet temperatures exceed T_f because $n \to 0$ in that case. This represents a limit toward stable equilibrium when the temperatures exceed the equilibrium phase change point. Conversely, all incoming liquid droplets are solidified on impact when the air temperatures become sufficiently low. In this case, $n \to 1$, and the droplets are solidified into the equilibrium stable state of solid on impact (rime ice), without any flowing supercooled film of metastable water. Thus, the formulation predicts the stable states of water in the upper and lower limiting trends of temperature and accommodation of both stable and metastable states in the region between those limits.

In Eq. (13), the collection efficiency (or impingement efficiency β) represents the surface's tendency of collecting droplets. As described earlier, it is calculated by the ratio of the actual droplet influx to the maximum influx that would occur on the surface, provided that the droplets were not deflected by the airstream. The collection efficiency is affected by the spatial distribution and size of droplets, airflow characteristics near the surface, near-wall forces such as gravity and drag forces, and other factors. The extent of droplet deflection by the airstream near the ice surface depends on the droplet inertia relative to the inertia of the local airstream. For example, small droplets (30 μm; in-flight icing) are often deflected away from the ice surface, whereas larger droplets (1 mm; freezing rain) have higher inertia relative to the same airstream, and so they are often scattered less before they impinge on the surface.

Some typical representative values of the collection efficiency will be considered, in terms of surface position, droplet size, and flow conditions. In this paper, constant collection efficiencies of 0.5 (average value) or 1 are used based on the parameters of the benchmark problems described by Myers and Hammond.[13] More generally, a local impingement calculation within the element could be performed as a postprocessing step after the local airflow is predicted because the multiphase flow is considered to be dilute, that is, less than 1% fraction of droplets in air, by volume. Such calculations would capture the spatial distribution of the collection efficiency, which is typically plotted in terms of position along the surface.

Two specific parameters of interest are the peak value and the impingement limit, that is, positions where the impingement ends. For example, Papadakis et al.[14] show local collection efficiencies for a Boeing 737 engine inlet at various circumferential locations. The peak value is 0.66 for a mean droplet diameter of 20 μ and an air velocity of 165 mph, whereas the impingement limits are observed at an angle of 180 deg. For the same surface location and inlet mass flow, the results show that larger values of the collection

efficiency and impingement limits occur for droplets with larger average diameters. In the following section, the numerical method for predicting such droplet and icing processes is presented.

III. Numerical Procedure

The numerical analysis is based on a control-volume-based finite element method (CVFEM), as previously developed for multiphase flows with droplets[4] but extended here to glaze ice problems. The main focus of this paper is to derive and apply the analytical modeling in the preceding section to the flowing supercooled surface film, for both stable and metastable states. The analytical model provides a locally one-dimensional approximation within a finite element along the ice surface. This approximation is consistent with the linear interpolation perpendicular to the ice interface, as performed by the bilinear interpolation of the CVFEM. (See sample finite element in Fig. 1.) The multidimensional effects are accommodated after all elements are assembled within the overall numerical formulation.

In the numerical formulation, an Eulerian approach is used to predict the motion of the carrier (air) and dispersed (droplet) phases in the freestream. In the near-wall region, where incoming droplets and phase change occur, the phase fractions of solid (ice), liquid (droplets, unfrozen water layer) and gas (air) are calculated simultaneously. This approach differs with other methods developed previously, such as that in Ref. 15. In previous methods, various limitations inherent in each formulation of rime/glaze ice growth have affected their performance capabilities. Unlike a single continuous parameter, n, described in Sec. II, discrete changes in procedural techniques for each regime can destabilize the computations, particularly during rime/glaze ice transition. Also, previous methods have often adopted a segregated approach, whereby the air and droplet flows are calculated, followed by ice accretion predictions. Then, a separate algorithm is used to move the ice boundary and perform remeshing of the domain, without a return to the energy equations and establishment of whether the domain change affects the rime/glaze ice transition. In the current work, a nonsegregated approach is used, whereby the equations are solved simultaneously to allow a fixed grid without remeshing at each time step.

The basis of this new approach involves the newly derived parameter of the freezing fraction of incoming droplets n, as outlined in Eq. (13). With this parameter, an Eulerian approach can properly reach the two-phase (rime ice) limit from three-phase (glaze ice) conditions when the temperatures are lowered sufficiently. It allows predictions of each regime separately, or simultaneously, with the transition therein. Because of its volume averaging approach, it differs with past Lagrangian methods involving explicit tracking of droplet trajectories, impact, and phase interface motion. Such methods can become very computationally intensive, as suggested by other technologies that have attempted to avoid such tracking through volume averaging. For example, groups of particles are often tracked in a quasi-Eulerian approach for particle image velocimetry (PIV), rather than individual particles.

Special consideration is needed for near-wall processes when modeled within an Eulerian framework. For example, locally one-dimensional analytical models (similar to the model described in Sec. II) could be incorporated within the near-wall elements to accommodate multidimensional splashing and surface roughness effects. The near-wall nodal and integration point variables, including droplet phase fraction, droplet and air velocities, and temperatures, are viewed to be capable of providing accurate estimates of such processes. Additional accuracy could be obtained by reduction of the mesh spacing near the wall. Alternatively, the importance of Lagrangian droplet tracking could be retained in the near-wall elements, where individual droplet processes are most essential, whereas computational savings could be realized through Eulerian volume averaging away from the wall. This approach would represent a type of hybrid Lagrangian/Eulerian method, which would focus on minimization of the computational time and storage, while still retaining the essential physical processes and accuracy therein. Because standard single-variable solvers could be used, that is, phase fraction of droplets, this method would have promising potential for realizing computational savings in terms of time and storage.

In the numerical formulation, the proportion of incoming droplets, n, changes to the solid phase, whereas separate variables are used to track the gas (air) and liquid (droplets/unfrozen layer) phase fractions. Heat transfer modeling at the liquid/air interface is documented in Refs. 11 and 16. When the solid phase fraction becomes unity, it indicates that the control volume is completely filled with ice due to solidified droplets. As a control volume changes phase from partially filled to completely filled, the amount of droplet influx into the partially filled volume may exceed the volume available. As a result, the volume becomes filled and the excess amount is transferred to the adjacent control volume for proper mass conservation.

However, the mass exchange presents certain computational difficulties when the phase interface movement is handled. In particular, the phase fraction is a bounded scalar between 0 and 1, yet a droplet influx into a nearly filled volume may surpass this bound. This condition may lead to numerical instability. Furthermore, in multidimensional flows, the limiting droplet influx in a subcontrol volume (Fig. 1) may not be directly known, due to its implicit dependence on mass flows to/from other subcontrol volumes. As a result, an implicit weighting factor is applied to the droplet influx to ensure that such inflow does not exceed the volume available.[4]

This weighting factor may be expressed in terms of the volume fraction of liquid within a control volume f_l, as follows:

$$\eta = 2 - \left[2 \Big/ \left(1 + f_l^{0.1}\right)\right] \tag{14}$$

When the control volume is filled ($f_l \to 0$), then $\eta \to 0$. Thus, when η is multiplied by the mass influx into a filled control volume, this influx is numerically damped to zero when the control volume becomes filled (as expected). In this way, mass flow into a control volume is implicitly blocked when it becomes filled. Without such blockage, the mass overflow would be realized after the solution, and either further iterations or mass redistribution (both time-consuming steps) would be needed. In the numerical solution, once $\eta \to 0$ for a filled control volume, the excess mass is deposited implicitly within the adjacent control volume(s). The predicted phase fraction from the solution of Eq. (4) ensures conservation of mass between these adjacent elements.

In addition to limiting the droplet influx, the approach serves other useful purposes. The scaling factor is not applied in the freestream, but it falls abruptly to zero along the ice surface when the liquid and/or ice fraction approaches unity. Thus, it retains the regular freestream equations, unless the control volume contains ice buildup. After the near-wall control volume is filled with solidified mass from the incoming droplets, the fluid flow equations are decoupled from the phase change. This reduces computational costs (time and storage), as compared with remeshing of the moving boundary at each time step. Along the ice surface, a zero main flow velocity is obtained. A separate momentum balance is solved for the flowing supercooled surface film (glaze ice), or a zero velocity is predicted in the rime ice. A droplet fraction is initially computed in the air/droplet control volume, and, if necessary (along the ice surface), another liquid fraction is computed in the three-phase control volume containing the unfrozen water layer.

A robust technique is required to identify the moving boundary, where impinging droplets are solidified and a flowing surface film is generated. Initially, the numerical algorithm searches for all external boundaries containing zero penetration (no-slip) boundary conditions. Then, the droplet influx perpendicular to these boundaries comprises a region where accretion of ice and/or droplets may occur. Only the flux component normal to the ice surface accumulates on the surface. Other accumulation, such as metastable film flow along the surface, occurs in addition to this incoming flux, and it is handled separately. Separate predictions are made for the air and droplet flow components.

This numerical formulation entails certain assumptions, summarized as follows. In particular, two-dimensional dilute flows with negligible droplet/droplet interactions are considered, with constant thermophysical properties for the ice, water, and air. The distribution of phases within each discrete control volume is assumed to be uniform, due to the volume averaging. The phase interface can move

within two adjacent control volumes (at most) in a single time step. Also, the effects of droplet splashing and breakup at the liquid/air interface are neglected. Based on the thin film approximation for the flowing supercooled surface film, a linear velocity profile is used therein. Constant coefficients of convection, evaporation, and collection efficiency have been considered at the ice surface, with negligible thermal effects of sublimation, viscous dissipation, and radiation. Furthermore, freezing of water in the surface film is assumed to occur at the equilibrium phase change point (0°C). In the following section, numerical results are presented for sample problems involving glaze ice growth.

IV. Results and Discussion

Consider a problem involving droplet flow and impact on a planar surface (Fig. 1). Droplets moving with the airflow impinge on the wall. During the initial stages of droplet impact, rime ice occurs such that impinging droplets are solidified immediately on impact. The coordinates are defined so that the incoming droplets are initially located at $y = 0$ (dimensionless coordinate) and so that they move toward the wall ($y = Y$) at a uniform velocity u. In this case, an analytical solution for the position of the ice/air interface, λ, can be written in terms of time t, impinging droplet velocity u, and volume fraction of droplets in the air C, that is,

$$\lambda = Y - [t - (Y/u)]uC \tag{15}$$

for $t \geq Y/u$. This result can be derived from a mass balance between the incoming droplets and the resulting accreted ice. Equation (15) recognizes that there is some time duration, Y/u, before the droplets arrive at the surface.

After the period of rime ice, transition occurs, and an unfrozen water layer is formed on the ice surface ($t > t_w$). Myers and Hammond[13] present an analytical solution of transient ice growth under glaze ice conditions with specified wall temperature boundary conditions. Although not explicitly outlined in the analytical solution, the numerical model must accommodate two dimensionality. Surface runoff occurs in the direction perpendicular to the incoming droplets (x direction), whereas the ice growth occurs in the y direction. The analytical solutions for the thickness of ice $B(t)$ and the water film $b(t)$ on a planar surface can be written as

$$\frac{\partial B}{\partial t} = \frac{a_2}{B} - \frac{a_3}{1 + a_1 b} \tag{16}$$

$$b = \frac{\beta V G}{\rho_w}(t - t_w) - \frac{\rho_i}{\rho_w}(B - B_w) \tag{17}$$

where a_1, a_2, and a_3 represent problem parameters involving air velocity and temperature. Also, the variables t_w and B_w refer to the time and thickness of ice at the transition point between rime and glaze ice. Values of these constants and parameters are derived and discussed by Myers and Hammond.[13]

In a graphic representation of the numerical results, phase fraction contours are used to represent the advancing ice interface as it grows into the incoming air direction. Contours of the non-air-phase fraction (that is, liquid droplets and/or ice) essentially track the droplet trajectories, as well as the ice accumulation on the surface. At the inflow boundary, a specified phase fraction is equivalent to a specified LWC. When Eqs. (4–6) are solved, the resulting phase fraction and droplet distributions can be tracked throughout the flowfield. Thus, useful processes such as droplet impingement and the collection efficiency of the surface can be predicted.

The phase fraction contours can depict the droplet movement throughout the domain, provided that the intervals between the phase fraction contours are sufficiently small. However, such refinement may be too fine to capture the larger magnitude of phase fractions at the solid boundary accompanying the growing ice interface. Thus, the contour labeling is specified within the order of magnitude of the LWC of freestream droplets (for the former case), or surface liquid/ice (for the latter case). In the currently reported results, the phase fraction contours are linear for ice accumulation on a planar surface. Thus, the results can be represented on a standard $B - t$ type graph.

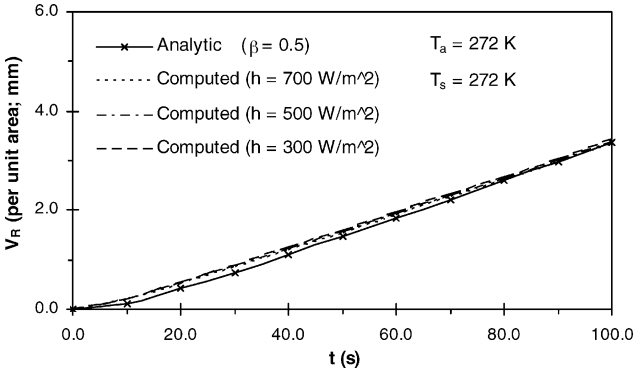

Fig. 2 Liquid runoff and convective heat transfer.

In Fig. 2, the volume of runoff of the flowing metastable layer (per unit area of surface) V_R is predicted based on a time-step size and grid spacing of 1.0 s and 0.5 mm, respectively. Such spatial and temporal discretizations were determined essentially to provide time-step and grid independence of results. The air temperature, surface temperature, air velocity, and ambient LWC are 272 K, 272 K, 90 m/s, and 0.001 kg/m^3, respectively. The liquid runoff in Fig. 2 represents the mass of incoming droplets that did not solidify on the ice surface but rather flowed off of the ice surface. It can be observed that close agreement is achieved between the analytical and predicted results. The results are determined after the difference between the glaze ice buildup and the dry growth limit is taken, corresponding to rime ice. As expected, because of the small temperature difference between T_f and T_a, the convective heat transfer is observed to have a negligible impact on the liquid runoff in Fig. 2. If V_R is multiplied by the water density, then the runback flow rate can be approximated by the slope of the nearly linear curve in Fig. 2. It can be verified that this slope approaches zero when the ambient air temperature is lowered sufficiently, that is, approaching the stable limit of dry growth.

Reasonable agreement with the analytical result is achieved in Fig. 2, but some discrepancy is observed, particularly at earlier stages of time. This discrepancy can be partly attributed to the underpredicted time of transition to glaze ice. For the flowing supercooled surface film, there exists a lack of relevant experimental data in the technical literature. The actual processes may vary with perturbations arising from impinging droplets, surface texture, and other factors, thereby making repeatability of detailed measurements difficult. Also, there exists considerable uncertainty in certain empirical coefficients themselves, such as the convective heat transfer coefficient.[1] As a result, the numerical modeling is mainly focused on the capabilities of predicting the overall trends.

The significance of the convective heat transfer coefficient h during ice growth has been considered by other researchers, for example, measurements of the coefficient by Van Fossen et al.[17] However, such measurements during glaze ice growth are difficult, and wide variations of the coefficients have been reported. Determination of what values should be used, and how they should vary temporally and spatially as a function of the surface characteristics, remains a challenging and significant problem in icing research. In particular, the detailed impact of such variations on the predicted ice shape and mass is not well understood in the technical literature.

For example, the convection coefficient has been reported in terms of power law coefficients, a and b, involving the Nusselt number.[17] Average coefficients such as $a = 0.2$ and $b = 0.82$ have been reported by Van Fossen et al.,[17] whereas Makkonen[18] uses $a = 0.032$ and $b = 0.85$, and Poots[10] suggests $a = 0.117$ and $b = 0.68$. Such variations generally do not consider the transient effects of the growing ice shape. Even convection coefficients for simpler (uniced) geometries, such as an uniced circular conductor, have limited accuracy ($\pm 25\%$; Ref. 1).

Fortunately, under certain conditions, such as those in Fig. 2, (that is, air and surface temperatures within 1°C of 273 K), these

uncertainties and variations in the convection coefficient have been observed to have minor overall effects. Figure 2 indicates that the results are not highly sensitive to a specific convection correlation under the given conditions, which is useful in view of the discrepancy of suggested correlations for such icing conditions in the literature. Under these conditions, the effects of other parameters can be evaluated without appreciable errors or uncertainties arising from the selected convection correlation.

Additional studies have been performed, so that other problem parameters leading to a minor effect of the convection coefficient h can be better understood. The maximum difference between analytical ice thicknesses at the end time in Fig. 2 ($t = 100$ s) over the range of h will be called the convection coefficient sensitivity. A small sensitivity percentage suggests that the effects of h are minor. When the difference between rime and glaze ice thicknesses is considered, this sensitivity also applies to the range of predicted liquid runoff results. When the air and surface temperatures are within 1°C of 273 K (reference case; $\Delta T = 1$ K), the sensitivity is about 4%. When the air temperature is lowered and within 10°C of 273 K, the sensitivity becomes higher at about 14%. The sensitivity remains less than about 10%, provided that the air temperature remains within about 9°C of 273 K.

A diminished sensitivity to h is observed with other problem parameters, such as the freestream LWC G and the collection efficiency β. For example, when the LWC is raised to $G = 0.002$ kg/m^3, the sensitivity factor becomes 2% for the initial reference case ($\Delta T = 1$ K). As expected, additional latent heat is released when the LWC is higher, and so it is expected that the role of convection is diminished. Also, the sensitivity factor for the reference case is reduced to 2% when the collection efficiency is raised to $\beta = 1$. As expected, kinetic energy of incoming droplets and cooling by these supercooled droplets on impact have higher contributions to the interfacial heat balance when β is higher, so that the role of convection is again diminished in that case.

In Fig. 3, reasonable agreement is achieved between analytical and predicted results of glaze ice buildup, particularly when the grid spacing is reduced. In Fig. 3, $T_a = 263$ K and $T_s = 263$ K are the values of air temperature and surface temperature, respectively (denoted Ta and Ts in Fig. 3). The dry growth limit is shown here for comparison purposes because it gives the maximum possible ice buildup as it occurs when all droplets are solidified immediately on impact. It represents an important validation limit because the predicted glaze ice buildup must not exceed the limit imposed by a mass balance in the dry growth limit. Close agreement between measured and analytical results for rime ice conditions has been demonstrated previously,[7] and so the dry growth limit is considered to represent the rime ice growth accurately in this work.

The grid spacing has a unique significance in the formulation of the new Eulerian method. For example, a discrete distance perpendicular to the phase interface was needed in Eq. (13), when the conduction heat flux and freezing fraction were approximated. This distance depends on the grid spacing. When the freezing fraction is calculated, special grid refinement at the phase interface(s) is not required. This offers useful advantages over other methods,[1] such

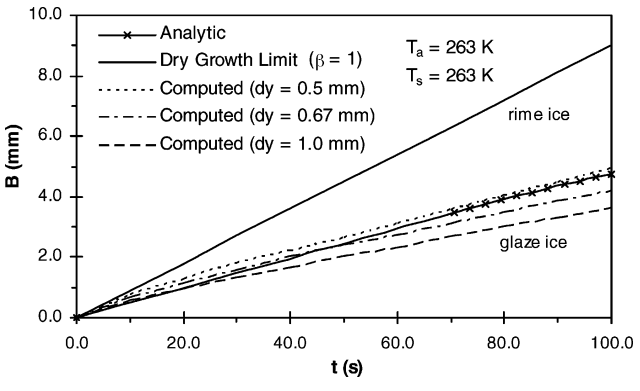

Fig. 3 Grid refinement study of predicted ice thickness.

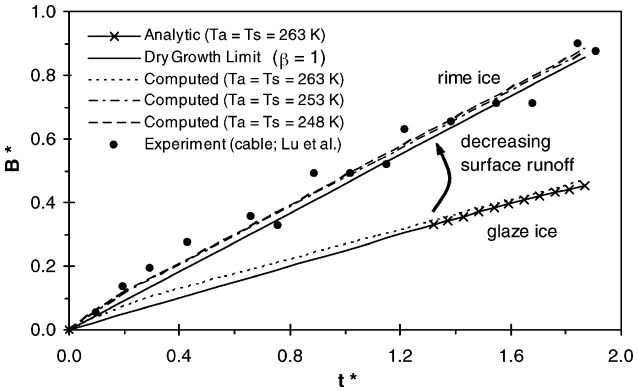

Fig. 4 Limiting trends near the dry growth limit.

as interface tracking, coordinate transformations, or k–ω turbulence models requiring detailed grid refinement near the wall (or phase interface) because remeshing after each time step could be avoided. As the phase interface passes across the boundary of a control volume within a time step, redistribution of the droplet influx between adjacent elements changes with different grid spacings. Such dependencies on the grid spacing are considered, through the overall impact on ice growth, in Fig. 3.

In Fig. 4, the results of Fig. 3 are extended to lower temperatures to validate the required trends toward the two-phase limit (rime ice). As expected, it can be observed that the predicted ice growth approaches the dry growth limit at temperatures of 253 K and lower. This properly establishes that the surface runoff and metastable film flow are reduced to zero in this limit. Slight discrepancies are observed between the predicted ice buildup and the dry growth limit. However, previous studies have shown similar deviations between predicted and measured data for rime ice growth.[7] Sample experimental data from those previous studies for iced circular conductors are shown in Fig. 4.

In Fig. 4, the nondimensional ice thickness B^* and nondimensional time t^* are defined as[4]

$$B^* = B/R \tag{18}$$

$$t^* = 2(\rho_w/\rho_i)(PNt/R) \tag{19}$$

where the precipitation rate is

$$P = VG/\rho_w \tag{20}$$

and R and N represent a reference length, that is, conductor radius, and surface projection view factor for the side of the object facing the incoming droplets,[5] respectively. For a circular conductor, $N = 1/\pi$, whereas $N = 1$ for a planar wall. This factor is needed because the projected widths of a circular conductor and planar wall are different due to surface curvature when the incoming mass flux of droplets is considered. For the two-dimensional problem of circular cable icing, B refers to the uniform ice thickness with the same equivalent mass as that actually observed.

Both one- and two-dimensional ice growth must approach the same dry growth limit, provided that the results are all nondimensionlized equivalently. The measured data are closely scattered about the dry growth limit, with certain deviations due to factors such as uncertainties in measurement of the precipitation rate and ice thickness.[7] In Fig. 4, the predicted results remain within this range where the experimental data are scattered. As a result, it appears that an Eulerian formulation of a flowing metastable water film will successfully approach the proper limiting trend (dry growth limit) when the air temperatures are lowered sufficiently.

Because the surface runoff is represented by the difference between the predicted ice buildup and the dry growth limit, Fig. 4 indicates that this metastable runback flow becomes zero when the air temperatures are lowered sufficiently. The proper asymptotic trends are observed from three-phase (glaze ice) to two-phase (rime ice) conditions. Thus, the freezing fraction in Eq. (13) provides a

new approach for modeling of stable and metastable states of the flowing surface film in an Eulerian framework. Stable equilibrium would be reached in regions without droplet impingement, where phase change would be governed by the local equilibrium freezing temperature. Also, metastable flow of water within the surface layer is predicted. Unlike Lagrangian tracking of the phase interface(s) or droplet trajectories, the current method utilizes volume averaging of the near-wall film flow for potential computational savings (time and storage). In the Eulieran approach, a single solution procedure and algebraic solver can be adopted for the dispersed (droplet) and continuous (air, flowing liquid film, ice) phases.

It was described that the freezing fraction of incoming droplets, Eq. (13), includes a combined heat and mass balance at the water/ice interface. In the heat balance, the conduction heat flux and temperature gradient within the unfrozen water layer are needed. This subelement temperature gradient represents a challenging part of the volume averaged calculations when the freezing fraction of incoming droplets is estimated. As a result, it was considered that validation against experimental data was important to assess the suitability of the use of such temperature gradients in the formulation. If the temperature gradient was determined to have an appreciable impact on the predicted ice growth, then it could be used as a relevant parameter when the freezing fraction of incoming droplets is predicted.

These comparisons against experimental data are illustrated in Fig. 5. The measured data were obtained in freezing rain experiments, as documented by Lu et al. for iced cables.[19] The predictions involve analysis[16] based on the modeling of glaze ice, as outlined in this paper. In Fig. 5, the liquid water content of air and freestream wind velocity are 0.00078 kg/m^3 and 5 m/s, respectively, whereas the ambient air temperature and surface heating rate are shown in Fig. 5. The results based on the full temperature gradient (denoted by M) within the unfrozen layer closely agree with the measured data. Errors when heat conduction in the unfrozen water layer is neglected, or inaccuracies of the predicted layer thickness or water/air interface temperature, lead to deviations of the temperature gradient in the water layer. Figure 5 shows that a 40% deviation (0.6*M) and a 60% deviation (0.4*M) of the temperature gradient M lead to errors in the predicted ice thickness.

These results suggest that heat conduction and the temperature gradient within the unfrozen layer have significance when the freezing fraction in Eq. (11) is predicted. From Eq. (11), the freezing fraction is expressed in terms of the temperature gradients on both sides of the ice/water interface. The temperature gradient within the ice is dependent on the interface temperature (assumed to be 0°C) and the wall temperature (dependent on the wall heating rate). Thus, the effects of temperature T_a and LWC G are observed through the other term in Eq. (11), namely, the temperature gradient within the surface film. Because those parameters (T_a and G) are expected largely to control the freezing fraction n, the film temperature gradient should exhibit a certain influence on the ice growth, if the freezing fraction model in Eq. (11) is considered to be physically realistic.

If the liquid layer was isothermal, then Eq. (11) would not properly predict the transition and growth of glaze ice. The film temperature gradient would be negligible in that case, and the predicted results would not be expected to vary with M. However, considerable variations are observed in Fig. 5, which suggests that the effects of M are not negligible. In particular, M contributes a nonzero value to Eq. (11). As a result, the equation is capable of predicting the range of conditions between $n = 1$ (rime ice, zero surface runoff) and $n = 0$ (complete surface runoff). Without such variations with M, the ice temperature gradient alone in Eq. (11) could not properly predict the freezing fraction of incoming droplets.

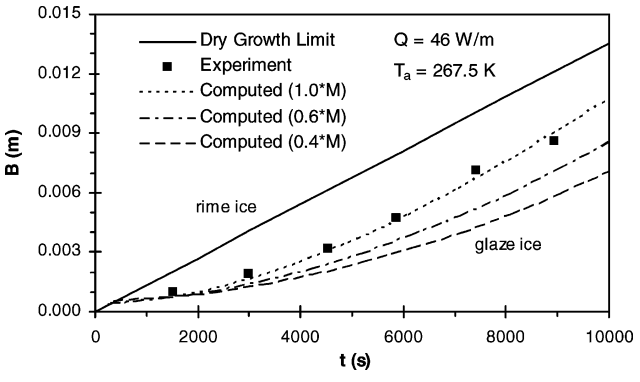

Fig. 5 Comparison between predicted and measured data.

V. Conclusions

In this paper, a new formulation is derived for the prediction of the metastable state of a flowing supercooled surface film. Unlike previous methods involving explicit tracking of the phase interface or droplet trajectories, the current approach derives a freezing fraction of incoming droplets with a volume averaging procedure. This method accommodates the coupled heat and momentum balances within the flowing surface layer. A main result is its ability to reach the expected asymptotic trends properly when the flow temperatures are lowered sufficiently. A newly defined parameter, called the freezing fraction of incoming droplets, predicts the liquid phase fraction over the range between three-phase (glaze ice) and two-phase (rime ice) conditions. The numerical simulations are performed with a CVFEM. Numerical predictions are successfully validated by comparisons with analytical solutions and measured data. The results indicate that an Eulerian volume averaging procedure can be successfully applied to three-phase conditions along the glaze ice surface, in contrast to Lagrangian methods used previously for such problems.

Appendix: Gibbs Free Energy of Supercooled Water Layer

Consider the phase change of water to ice at the equilibrium point of $T_f = 273.15$ K. The enthalpy and entropy of fusion due to this phase transformation are given by[1]

$$\Delta H_f = -6.007\ KJ \tag{A1}$$

$$\Delta S_f = \Delta H_f / T_f = -6.007/273.15 = -21.99\ J/K \tag{A2}$$

where the subscript f refers to the phase change point.

The entropy of fusion indicates the entropy change of the system due to freezing. The total entropy change (system and surroundings) can be expressed in terms of the change of Gibbs free energy, as follows:

$$\Delta S_{\text{tot}} = -(\Delta \hat{G}/T) \tag{A3}$$

where, in this case,

$$\Delta \hat{G}_f = \Delta H_f - T_f \Delta S_f = -6.007 - (273.15)(-21.99) = 0 \tag{A4}$$

Because of this zero change of the Gibbs free energy, the freezing process is reversible. Although this result is consistent with the stable equilibrium of water and ice at 273.15 K, the actual phase change during surface icing is not considered to be reversible. Thus, the temperature within the unfrozen layer will be considered to be greater than or less than T_f.

For the water layer along the ice surface, it is considered that the water was cooled below the freezing point by the impinging supercooled droplets. Assume that the enthalpy and entropy of fusion are independent of temperature near the equilibrium freezing point. Also, consider that the water has been cooled to a temperature of $T_{f,m}$, which is below the equilibrium point of T_f. Thus, by calculation of the change of Gibbs free energy and comparson with Eq. (24),

$$\Delta \hat{G}_{f,m} = \Delta H_{f,m} - T_{f,m} \Delta S_{f,m} < \Delta \hat{G}_f \tag{A5}$$

In this case, the change of Gibbs free energy for the supercooled water becomes negative. The stable equilibrium point at

T_f corresponds to a global minimum of $\hat{G}$, and so this negative change of $\Delta\hat{G}_{f,m}$ suggests a metastable state with a local minimum of the Gibbs free energy. A free energy barrier between the metastable and stable states sustains the supercooled water until it contacts a suitable nucleation site to initiate freezing on the ice surface.

Because $\Delta\hat{G}_{f,m} < 0$ from Eq. (25), the total entropy change in Eq. (23) becomes positive. Thus, based on the second law of thermodynamics, the freezing of the supercooled water is irreversible and spontaneous, and the negative temperature gradient in Eq. (10) becomes possible. Similar calculations for temperatures above T_f would give positive values of $\Delta\hat{G}$, leading to negative values of ΔS_{tot}. A positive value of $\Delta\hat{G}$ implies a nonspontaneous process, whereby work input is required (such as work corresponding to the kinetic energy of impinging droplets).

Acknowledgments

Financial support from the Natural Sciences and Engineering Research Council of Canada and Westland Helicopters, Ltd., is gratefully acknowledged.

References

[1]Naterer, G. F., *Heat Transfer in Single and Multiphase Systems*, CRC Press, Boca Raton, FL, 2002, Chaps. 9 and 11.

[2]Bragg, M. B., "Aircraft Icing," *Yearbook of Science and Technology*, McGraw–Hill, New York, 1999, pp. 183–185.

[3]Tsuboi, K., and Kimura, S., "Numerical Study of the Effect of Droplet Distribution in Incompressible Droplet Flows," AIAA Paper 98-2561, 1998.

[4]Naterer, G. F., "Multiphase Flow with Impinging Droplets and Airstream Interaction at a Moving Gas/Solid Interface," *International Journal of Multiphase Flow*, Vol. 28, No. 3, 2002, pp. 451–477.

[5]Naterer, G. F., Deng, H., and Popplewell, N., "Predicting and Reducing Glaze Ice Accretion on Electric Power Lines with Joule Heating: Theory and Experiments," *CSME Transactions*, Vol. 23, No. 1A, 1999, pp. 51–70.

[6]Messinger, B. L., "Equilibrium Temperature of an Unheated Icing Surface as a Function of Air Speed," *Journal of the Aeronautical Sciences*, Vol. 20, 1953, pp. 29–42.

[7]Lu, M. L., Popplewell, N., Shah, A. H., Barrett, W., and Au, A., "Mass of Ice Accretion from Freezing Rain Simulations," *Proceedings, Eighth International Workshop on Atmospheric Icing of Structures*, Reykjavik, Iceland, 1998.

[8]Yamaguchi, Y., Hansman, R. J., and Kazmierczak, M., "Deterministic Multi-Zone Ice Accretion Modeling," AIAA Paper 91-0265, Jan. 1991.

[9]Hansman, R. J., and Kirby, M. S., "Comparison of Wet and Dry Growth in Artificial and Flight Icing Conditions," *Journal of Thermophysics and Heat Transfer*, Vol. 1, No. 3, 1987, pp. 215–221.

[10]Poots, G., *Ice and Snow Accretion on Structures*, Wiley, New York, 1996.

[11]Naterer, G. F., "Eulerian Three-Phase Formulation with Coupled Droplet Flow and Multimode Heat Transfer," *Numerical Heat Transfer B*, Vol. 43, No. 4, 2003, pp. 331–352.

[12]Cheremisinoff, N. P., and Davis, E. J., "Stratified Turbulent–Turbulent Gas–Liquid Flow," *AIChE Journal*, Vol. 25, 1979, pp. 48–56.

[13]Myers, T. G., and Hammond, D. W., "Ice and Water Film Growth from Incoming Supercooled Droplets," *International Journal of Heat and Mass Transfer*, Vol. 42, 1999, pp. 2233–2242.

[14]Papadakis, M., Elangovan, R., Freund, G. A., and Breer, M. D., "Water Droplet Impingement on Airfoils and Aircraft Engine Inlets for Icing Analysis," *Journal of Aircraft*, Vol. 28, No. 3, 1991, pp. 165–174.

[15]Louchez, P., Fortin, G., Mingione, G., and Brandi, V., "Beads and Rivulets Modelling in Ice Accretion on a Wing," AIAA Paper 98-0489, Jan. 1998.

[16]Naterer, G. F., "Coupled Liquid Film and Solidified Layer Growth with Impinging Supercooled Droplets and Joule Heating," *International Journal of Heat and Fluid Flow*, Vol. 24, No. 2, 2003, pp. 223–235.

[17]Van Fossen, G. J., Simoneau, R. J., Olsen, W. A., and Shaw, R. J., "Heat Transfer Distributions Around Nominal Ice Accretion Shapes Formed on a Cylinder in the NASA Lewis Icing Research Tunnel," AIAA Paper 84-0017, 1984.

[18]Makkonen, L., "Modeling of Ice Accretion on Wires," *Journal of Climate and Applied Meteorology*, Vol. 23, 1984, pp. 929–939.

[19]Lu, M., Popplewell, N., Shah, A. H., Deng, H., and Naterer, G. F., "A Semi-Empirical Icing Model for an Energized Power Line," Dept. of Mechanical and Industrial Engineering, Internal Rept., Univ. of Manitoba, Winnipeg, Manitoba, Canada, 1999.

S. K. Aggarwal
Associate Editor